Generating Synthetic Computed Tomography and Synthetic Magnetic Resonance (sMR: sT1w/sT2w) Images of the Brain Using Atlas-Based Method

Fariba Farhadi Birgani[1], Mohamad Javad Tahmasebi Birgani[2], Roghayeh Kamran Samani[3], Fatemeh Maghsoodinia [3*]

1. Department of Medical Physics, Ahvaz Jundishapur University of Medical Sciences, Ahvaz, Iran
2. Radiation Therapy and Medical Physics Department, Golestan Hospital, Jundishapur University of Medical Sciences, Ahvaz, Iran
3. Department of Medical Physics, School of Medicine, Isfahan University of Medical Sciences, Isfahan, Iran

A R T I C L E I N F O	A B S T R A C T
	Introduction: Nowadays, magnetic resonance imaging (MRI) in combination with computed-tomography (CT) is increasingly being used in radiation therapy planning. MR and CT images are applied to determine the target volume and calculate dose distribution, respectively. Since the use of these two imaging modalities causes registration uncertainty and increases department workload and costs, in this study, brain synthetic CT (sCT) and synthetic MR (sMR: sT1w/sT2w) images were generated using Atlas-based method; consequently, just one type of image (CT or MR) is taken from the patient. *Material and Methods:* The dataset included MR and CT paired images from 10 brain radiotherapy (RT) patients. To generate sCT/sMR images, first each MR/CT Atlas was registered to the MR/CT target image, the resulting transformation was applied to the corresponding CT/MR Atlas, which created the set of deformed images. Then, the deformed images were fused to generate a single sCT/sMR image, and finally, the sCT/sMR images were compared to the real CT/MR images using the mean absolute error (MAE). *Results:* The results showed that the MAE of sMR (sT1w/sT2w) was less than that of sCT images. Moreover, sCT images based on T1w were in better agreement with real CT than sCT-based T2w. In addition, sT1w images represented a lower MAE relative to sT2w. *Conclusion:* The CT target image was more successful in transferring the geometry of the brain tissues to the synthetic image than MR target.

Introduction

Magnetic resonance imaging (MRI) and computed tomography (CT) are two complementary medical imaging techniques for various organs [1, 2]. The superiority of CT and MR images in clinical applications depends on the imaging goal and the target organ. MRI is the modality of choice for visualizing the details of brain tissues (e.g., gray matter, white matter, cerebrospinal fluid (CSF)) and brain tumors [3, 4]. In addition to displaying anatomical structures, MRI also provides physiological and metabolic information [5]. However, it has some disadvantages like long scan time and application restrictions such as emergency cases and patients with implanted medical devices [6, 7].

CT-scan also has its intrinsic advantages and drawbacks. CT scan of the brain is used in cases of bone fracture, trauma, and presence of foreign metal objects, infection, bleeding, and cerebrovascular accident [8-10]. This technique has a shorter scan time than MRI and therefore has less sensitivity to patient movement during examination. It also does not have the limitation of presence of ferromagnetic objects in the body. Since X-ray is used to produce CT images, the main concern in this imaging modality is patient's protection from radiation [11].

Radiation therapy planning (RTP) is one of the clinical applications used in both CT scan and MRI. MR and CT images are applied to determine the target volume and calculate dose distribution, respectively [3, 12, 13]. In order to transfer the organs and tumor delineations from MR to CT image, the two scans must be registered and fused, which results in a registration error of about 2 mm. This error causes a systematic shift in the delineations and leads to target under-dosage or over-dosage adjacent organs at risk (OAR). In addition, these imaging modalities increases department workload and costs [14-18].

*Corresponding Author: Email: f.maghsood@gmail.com

In this study, synthetic CT and synthetic MR (sMR: sT1w/sT2w) images of the brain were created using Atlas-based method; consequently, just one type of image (CT or MR) is taken from the patient.

Materials and Methods

In this method, the steps for creating a synthetic CT/MR are: (1) collect an Atlas MRI and CT dataset, (2) register each Atlas image to the target image (3), apply the displacement vector field (DVF) to the corresponding Atlas image, and (4) fuse the collection of deformed images into a single synthetic CT/MR (Table 1). In the following, each of these steps is detailed separately.

Table 1. The generation steps of synthetic computed tomography and magnetic resonance images

Synthetic CT	Synthetic MR (sT1w/sT2w)
1.Collect an Atlas database (CT/MR pairs)	
2a. Register each atlas T1w to the target T1w.	2. Register each atlas CT to the target CT.
2b. Register each atlas T2w to the target T2w.	3a. Apply same DVF to the atlas T1w.
3. Sum two DVF to generate a single DVF.	3b. Apply same DVF to the atlas T2w.
4. Apply single DVF to the atlas CT.	4a. Fuse the set of deformed T1s.
5. Fuse the set of deformed CTs.	4b. Fuse the set of deformed T2s

DVF: displacement vector field

Atlas dataset collection

In this study, dataset consists of MR and CT paired images from 10 brain radiotherapy (RT) patients. The corresponding CT images were acquired with a Siemens Sensation 64 with tube voltage of 120 kv, exposure of 150 mAs, in-plane resolution of 0.5×0.5 mm^2, and slice thickness of 1 mm. The MR images were obtained by 1.5 T Magnetom Essenza (Siemens, Germany). The MR sequences were gradient echo T1-weighted (TE/TR = 4.5/1700, voxel resolution $1 \times 1 \times 1$ mm^3, field of view 512×512, and flip angle 20°) and gradient echo T2-weighted (TE/TR = 107/500 and the rest of its parameters were similar to gradient echo T1-weighted). Sample size calculation and patient selection were based on Sjölund et al. study [19].

To create Atlas MR and CT images, an image pre-processing step was performed, which included removing the noise with the Gaussian filter and separating the image background from the brain with morphological operators. Then, each MRI and CT pair was resampled and registered rigidly using mutual information. The rigid registration using mutual information is one of the forms of linear transformation models. It is an intensity-based method comparing intensity patterns in images via correlation metrics. In order to register CT and MR images, the moving image (CT), the fixed image (MRI), and metric parameter were specified. The transformation matrix that maps points in moving image to the corresponding points in fixed image was applied to the moving image to align it with the fixed image.

Displacement fields estimation

Since Atlas-based methods strongly depend on the correct and accurate registration between Atlas and target images, selecting a precise non-rigid (deformable) registration method is essential. Demons algorithm is used to find DVF to map Atlas image to the target image. Demons algorithm is a popular algorithm for non-rigid image registration because of its linear computational complexity and ease of implementation in MATLAB R2015a software. It approximately solves the problem of large geometric differences by successively estimating force vectors that correspond to the vibrational derivative of the dissimilarity measure and smoothing the force vectors by Gaussian convolution [20, 21]. Demons algorithm estimates the displacement field by aligning the target with Atlas image.

If the target image size is m×n, the output of Demons is two matrices m×n, where the first matrix represents displacement values along the x axis and the second matrix denotes displacement values along the y axis. The displacement values are in pixel. The obtained displacement fields are applied to the corresponding Atlas image.

As shown in Table 1, to generate a sCT image, two displacement fields (DVF-T1w and DVF-T2w) were gathered, and the combined DVF was applied to the corresponding Atlas CT image. However, to create sMR images (sT1w and sT2w), only one target (CT image) was used; hence, DVF was the same for both.

Deformed images fusion

Deformed images were generated after applying the displacement fields to the corresponding Atlas images. Then, they were fused to produce a single synthetic CT or synthetic MR image. We used the method presented by Sjölund et al. [19] to fuse the deformed images; in this method, the set of deformed images are registered to their joint mean.

Evaluation

To compare synthetic CT/MR with real CT/MR images, the mean absolute error (MAE) measurement was used. MAE is the simplest and most common measure in synthetic CT studies. Since CT and MR images are fused to transfer MR delineations to CT for radiotherapy purposes, the fused images were also evaluated. The MAEs of sCT, sMR (sT1w/sT2w), and fused images are calculated as [15, 19]:

$$MAE = \frac{1}{N}\sum_{i=1}^{N}\left|HU_{CT}(i) - HU_{sCT}(i)\right| \quad (1)$$

$$MAE = \frac{1}{N}\sum_{i=1}^{N}\left|SI_{T2w}(i) - SI_{sT2w}(i)\right| \quad (2)$$

$$MAE = \frac{1}{N}\sum_{i=1}^{N}\left|SI_{T1w}(i) - SI_{sT1w}(i)\right| \quad (3)$$

$$MAE = \frac{1}{N}\sum_{i=1}^{N}\left|PI_{fusion(CT \& T1w)}(i) - PI_{fusion(CT \& sT1w)}(i)\right| \quad (4)$$

$$MAE = \frac{1}{N}\sum_{i=1}^{N}\left| PI_{fusion(CT\,\&T\,2w)}(i) - PI_{fusion(CT\,\&sT\,2w)}(i) \right| \quad (5)$$

where N is the total number of voxels inside the outline of MR or CT. HU, SI, and PI represent the Hounsfield unit (HU) values of the CT and sCT, signal intensity (SI) values of the MR and sMR, and pixel brightness intensity (PI) values of the fused images at the corresponding spatial positions, respectively.

All the mentioned processes were run in MATLAB R2015a.

Results

The synthetic CT images based on two MR targets (the sum of T1w DVF and T2w DVF) and the synthetic T1 and synthetic T2 images based on CT were generated. In Figure 1, the sCT and sMR (sT1w/sT2w) images related to a specific slice of a patient are displayed.
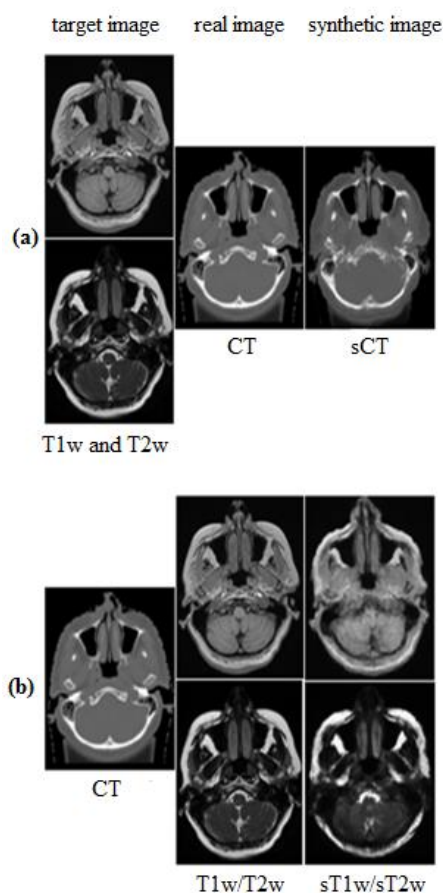

Figure 1. Example of the generated sCT (a), sT1w and sT2w (b) images

As shown in Table 2, the MAEs of synthetic CT images were 62.3±9.5 HU, 78±13.7 HU, and 83 ±19.7 HU for the two T1w/T2w targets, only T1w, and only T2w target, respectively. The sCT images generated by two targets (T1w and T2w) showed less error than one target (T1w or T2w). As previously mentioned, the same CT target was used to create sMR images; and the

MAEs were 47±7.3 SI for sT1w and 52±9.1 SI for sT2w. In radiotherapy, in order to transfer delineations from MRI to CT, these images are fused together. MAE was also calculated for the real CT and sMR fused images. The MAEs were 2.5±0.2 PI and 2.6±0.2 PI for the CT/sT1w and CT/sT2w fused images, respectively.

Table 2. Mean absolute error of the synthetic computed tomography and synthetic magnetic resonance images for 10 brain patients

Images	MAE (HU/SI/PI *)
sCT (based T1w and T2w)	62.3±9.5 HU
sCT (based only T1w)	78±13.7 HU
sCT (based only T2w)	83 ±19.7 HU
sT1w	47±7.3SI
sT2w	52±9.1SI
Fusion real CT and sT1w	2.5±0.2 PI
Fusion real CT and sT2w	2.6±0.2 PI

* Hounsfield Unit (HU), Signal Intensity (SI), Pixel Intensity (PI), MAE: mean absolute error

For further analysis, regions of interest (ROIs) in real CT/real MR and sCT/sMR images were selected in seven regions (i.e., bone, soft tissue, air, tumor, soft tissue-bone, air-soft tissue, and air-bone boundaries). In order to reduce the uncertainty caused by Gaussian noise, the ROIs were circulars with a diameter of 5 mm [12]. MAEs of each region are shown in Table 3. The lowest MAE was related to soft tissue (18±5.2HU), bone (12±2.4) and tumor (13±4.3) in sCT, sT1w and sT2w, respectively.

Table 3. Average mean absolute error of regions of interest in seven regions

ROIs	Mean MAE (HU) sCT (based T1w and T2w)	Mean MAE (SI) sT1w	Mean MAE (SI) sT2w
bone	68±12.3	12±2.4	18±4.6
Soft tissue	18±5.2	34±6.7	44±9.8
air	47±9.1	18. ±4.1	15±3.9
Soft tissue-bone boundary	52±8.9	28±5.7	31±7.7
Air-soft tissue boundary	61.6±10.2	26±4.6	29±5.6
Air-bone boundary	77±11.4	23.4.1	25±4.8
tumor	23±5.2	16±5.1	13±4.3

ROI: region of interest
MAE: mean absolute error

The average run time for generating sCT, sT1w and sT2w using a Core i5 PC system is shown in Table 4. The run time was calculated 13±3.2 min and 9±0.6 min for sCT based on one and two targets, respectively. This time for creating sT1w and sT2w was the same (10±0.8 min).

Table 4. Computing time to generate sCT and sMR images (min)

	sCT based T1w or T2w	sCT based T1w and T2w	sT1w/ sT2w based CT
Average	9	13	10
SD	0.6	3.2	0.8

Discussion

In this study, synthetic CT and MR images were generated by Atlas-based method. The results showed that the MAE of synthetic MR was less than that of synthetic CT images (Table 2). As a general conclusion, the CT target image appears to be more successful in transferring the geometry of the brain tissue to the synthetic MR image than MRI target.

Considering the capability of MRI to detect soft tissue, it is possible that a more complete description could be obtained by summing the DVFs of the two MR sequences (T1w and T2w) for creating the sCT. In the Atlas-based method, just one target (T1w or T2w) for generating sCT is often employed [22, 23], but this study used two pieces of target information (DVF-T1w and DVF-T2w). The results showed that the MAE of sCT based on the two targets (T1w and T2w) is lower than that of sCT based on one MR target (T1w or T2w).

By reviewing previous studies related to the three common Atlas methods (i.e., patch, deformable and hybrid), the range of MAE for brain was obtained between 85-114 HU [4, 15, 19, 24-26]. The produced sCT with patch-based method has the best agreement with the real CT; the MAE of this method using T1w target was calculated 85 HU [17]. Unfortunately, the patch-based method has a serious problem as it is heavily dependent on anatomical similarity, which affects the accuracy of the sCT, especially in tumors or other brain abnormalities.

The MAEs of deformable and hybrid (deformable and patch) methods were calculated 113.4 HU using Morphon deformable algorithm [19] and 101 HU [27],

respectively, with T1w target. In addition, the average MAEs for the multi-modal and multi-scale methods were calculated 118.7 ± 10.4 HU and 99.69±11.07HU [28], respectively, using an MR target. We also obtained the MAE to be 62.3±9.5 HU with two targets; however, sCTs generated by one target were also in agreement with previous studies. The feasibility of using T1w and T2w as targets for generating sCT in the brain was investigated, and the MAE for sCT was 124 ± 10HU [29]. We obtained an MAE of 62.3±9.5 HU with two targets; however, sCTs generated by one target yielded better results than previous studies.

The ROIs results showed that CT target has a better performance in transferring the geometry of air and air-bone boundary to sT2w than sT1w. A remarkable point in Table 3 is the tumor's declining MAE in the sT2w ROIs. This is because brain tumors are usually accompanied by edema, and edema in T2w has a stronger signal than T1w. In contrast, sT1w images were more effective in describing bone information due to higher signal of solid in T1w than T2w. Moreover, for sCT, the highest MAE was related to air-bone boundary, which is visually displayed in Figure 2.

The fused images of real CT and sT1w/sT2w were compared with real CT and real T1w/T2w. The obtained MAEs had slight differences (Table 2). In Figure 3, a sT1 (Fig.3.c1) and a sT2 (Figure 3.c2) images generated by CT target (Figure 3.a) are displayed. The fused images were subtracted (Figure 3. f1, f2), which showed differences in low intensity related to the dark areas of the image. These differences can be attributed to noise.
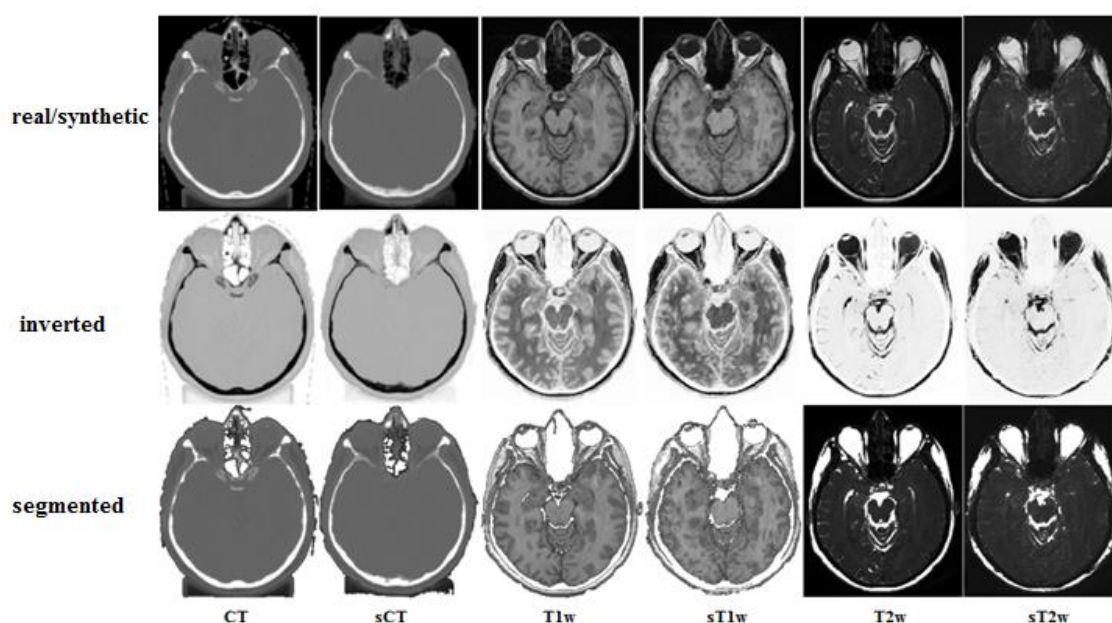

Figure 2. Inverted and segmented images of real and synthetic computed tomography and magnetic resonance imaging
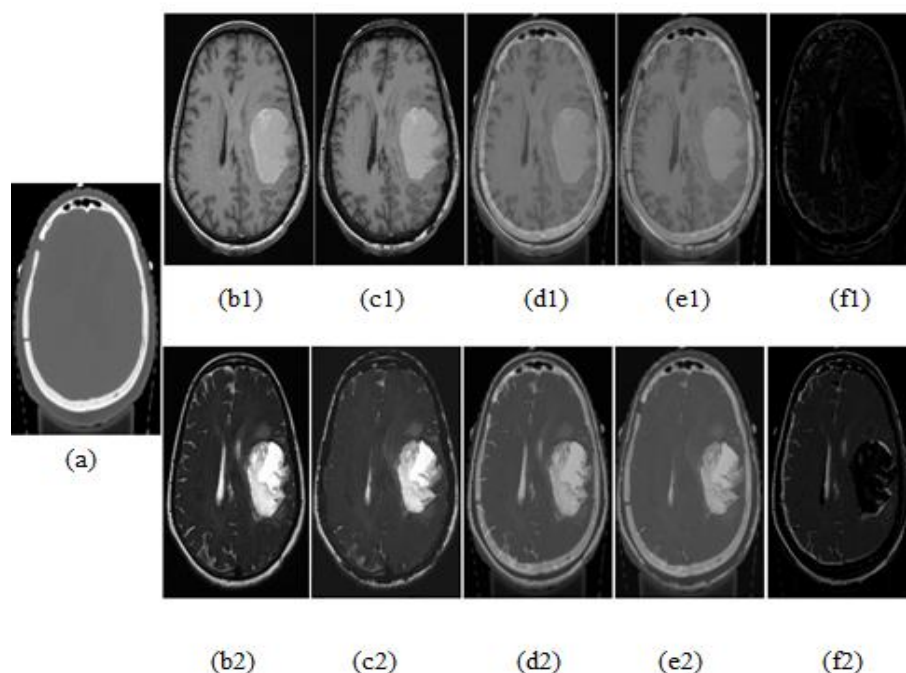
Figure 3. Synthetic magnetic resonance images generated by computed tomography (CT) target (a) related to specific slice: real T1w (b1), real T2w (b2), sT1w (c1), sT2w (c2), CT and T1w fused image (d1), CT and T2w fused image (d2), CT and sT1 fused image (e1), CT and sT2 fused image (e2), the image subtraction of d1 and e1 (f1) and the image subtraction of d2 and e2 (f2).

The run time to generate sCT image was about 13±3.2 min on a Core i5 PC system, which is less than the time reported by other studies (about 25, 16 and 38 minutes) [4,15,30]. The Demons algorithm demonstrated a high capability for MR-MR and CT-CT registration and a fast run time to generate sCT and sMR images.

There are no reports related to sMR creation. The innovation of our study is the use of an algorithm to create both sCT and sMR images. The advantages of the proposed study include 1) saving time and cost because only one image (CT or MR) is taken from the patient, 2) reducing the registration error because the synthetic image geometry is completely based on the target image, and 3) being applicable for patients with imaging restrictions such as CT restriction for pregnant women and MRI restriction for patients with implantable medical devices.

Conclusion

This study proposed a fast and precise algorithm to generate synthetic CT and synthetic MR images using Atlas-based approach, which could potentially be useful for radiotherapy treatment planning system. This study concluded that using the sum of two DVFs (DVF-T1w and DVF-T2w) is more accurate for generating sCT, and the CT target image is more successful in transferring the geometry of the brain tissues to the synthetic MR image. In addition, the sT2w images were more effective in describing tumor information due to the presence of edema in most brain tumors. In contrast,

sT1w images were more powerful in transferring bone geometry due to higher signal of solid in T1w than T2w.

Acknowledgment

References

1. Khoo V, Joon D. New developments in MRI for target volume delineation in radiotherapy. The British journal of radiology. 2006;79(1):S2-S15.
2. Sciarra A, Barentsz J, Bjartell A, Eastham J, Hricak H, Panebianco V, et al. Advances in magnetic resonance imaging: how they are changing the management of prostate cancer. European urology. 2011;59(6):962-77.
3. Gustafsson C, Nordström F, Persson E, Brynolfsson J, Olsson L. Assessment of dosimetric impact of system specific geometric distortion in an MRI only based radiotherapy workflow for prostate. Physics in Medicine & Biology. 2017;62(8):2976.
4. Uh J, Merchant TE, Li Y, Li X, Hua C. MRI-based treatment planning with pseudo CT generated through atlas registration. Medical physics. 2014;41(5).
5. Seitz M, Shukla-Dave A, Bjartell A, Touijer K, Sciarra A, Bastian PJ, et al. Functional magnetic resonance imaging in prostate cancer. European urology. 2009;55(4):801-14.
6. Rodriguez A. Principles of magnetic resonance imaging. Revista mexicana de física. 2004;50(3):272-86.

7. Van Reeth E, Tham IW, Tan CH, Poh CL. Super-resolution in magnetic resonance imaging: A review. Concepts in Magnetic Resonance Part A. 2012;40(6):306-25.

8. Saboori M, Ahmadi J, Farajzadegan Z. Indications for brain CT scan in patients with minor head injury. Clinical neurology and neurosurgery. 2007;109(5):399-405.

9. Noyola DE, Demmler GJ, Nelson CT, Griesser C, Williamson WD, Atkins JT, et al. Early predictors of neurodevelopmental outcome in symptomatic congenital cytomegalovirus infection. The Journal of pediatrics. 2001;138(3):325-31.

10. Von Kummer R, Bourquain H, Bastianello S, Bozzao L, Manelfe C, Meier D, et al. Early prediction of irreversible brain damage after ischemic stroke at CT. Radiology. 2001;219(1):95-100.

11. Hyatt AP. Computed tomography: physical principles, clinical applications, and quality control. Radiography. 2009;15(4):357-8.

12. Korhonen J, Kapanen M, Keyriläinen J, Seppälä T, Tenhunen M. A dual model HU conversion from MRI intensity values within and outside of bone segment for MRI-based radiotherapy treatment planning of prostate cancer. Medical physics. 2014;41(1).

13. Mazzara GP, Velthuizen RP, Pearlman JL, Greenberg HM, Wagner H. Brain tumor target volume determination for radiation treatment planning through automated MRI segmentation. International Journal of Radiation Oncology· Biology· Physics. 2004;59(1):300-12.

14. Eilertsen K, Nilsen Tor Arne Vestad L, Geier O, Skretting A. A simulation of MRI based dose calculations on the basis of radiotherapy planning CT images. Acta Oncologica. 2008;47(7):1294-302.

15. Andreasen D, Van Leemput K, Hansen RH, Andersen JA, Edmund JM. Patch-based generation of a pseudo CT from conventional MRI sequences for MRI-only radiotherapy of the brain. Medical physics. 2015;42(4):1596-605.

16. Dowling JA, Lambert J, Parker J, Salvado O, Fripp J, Capp A, et al. An atlas-based electron density mapping method for magnetic resonance imaging (MRI)-alone treatment planning and adaptive MRI-based prostate radiation therapy. International Journal of Radiation Oncology· Biology· Physics. 2012;83(1):e5-e11.

17. Lee YK, Bollet M, Charles-Edwards G, Flower MA, Leach MO, McNair H, et al. Radiotherapy treatment planning of prostate cancer using magnetic resonance imaging alone. Radiotherapy and oncology. 2003;66(2):203-16.

18. Johansson A, Karlsson M, Yu J, Asklund T, Nyholm T. Voxel-wise uncertainty in CT substitute derived from MRI. Medical physics. 2012;39(6Part1):3283-90.

19. Sjölund J, Forsberg D, Andersson M, Knutsson H. Generating patient specific pseudo-CT of the head from MR using atlas-based regression. Physics in Medicine & Biology. 2015;60(2):825.

20. Pennec X, Cachier P, Ayache N, editors. Understanding the "demon's algorithm": 3D non-rigid registration by gradient descent. International Conference on Medical Image Computing and Computer-Assisted Intervention; 1999: Springer.

21. Cahill ND, Noble JA, Hawkes DJ, editors. A demons algorithm for image registration with locally adaptive regularization. International Conference on Medical Image Computing and Computer-Assisted Intervention; 2009: Springer.

22. Edmund JM, Nyholm T. A review of substitute CT generation for MRI-only radiation therapy. Radiation Oncology. 2017;12(1):28.

23. Hsu S-H, Cao Y, Huang K, Feng M, Balter JM. Investigation of a method for generating synthetic CT models from MRI scans of the head and neck for radiation therapy. Physics in Medicine & Biology. 2013;58(23):8419.

24. Stanescu T, Jans H, Pervez N, Stavrev P, Fallone B. A study on the magnetic resonance imaging (MRI)-based radiation treatment planning of intracranial lesions. Physics in Medicine & Biology. 2008;53(13):3579.

25. Schreibmann E, Nye JA, Schuster DM, Martin DR, Votaw J, Fox T. MR-based attenuation correction for hybrid PET-MR brain imaging systems using deformable image registration. Medical physics. 2010;37(5):2101-9.

26. Kops ER, Hautzel H, Herzog H, Antoch G, Shah NJ. Comparison of template-based versus CT-based attenuation correction for hybrid MR/PET scanners. IEEE Transactions on Nuclear Science. 2015;62(5):2115-21.

27. Hofmann M, Steinke F, Scheel V, Charpiat G, Farquhar J, Aschoff P, et al. MRI-based attenuation correction for PET/MRI: a novel approach combining pattern recognition and atlas registration. Journal of nuclear medicine. 2008;49(11):1875.

28. Aouadi S, Vasic A, Paloor S, Torfeh T, McGarry M, Petric P, et al. Generation of synthetic CT using multi-scale and dual-contrast patches for brain MRI-only external beam radiotherapy. Physica Medica. 2017;42:174-84.

29. Pileggi G, Speier C, Sharp GC, Izquierdo Garcia D, Catana C, Pursley J, et al. Proton range shift analysis on brain pseudo-CT generated from T1 and T2 MR. Acta Oncologica. 2018:1-11.

30. Chen S, Quan H, Qin A, Yee S, Yan D. MR image-based synthetic CT for IMRT prostate treatment planning and CBCT image-guided localization. Journal of applied clinical medical physics. 2016;17(3):236-45.